2014

Synthesis and Characterization of a Plasmonic−Semiconductor Composite Containing Rationally Designed, Optically Tunable Gold Nanorod Dimers and Anatase TiO2

Mangelson, Bryan F.

CHEMISTRY OF MATERIALS

Article

pubs.acs.org/cm

Synthesis and Characterization of a Plasmonic–Semiconductor Composite Containing Rationally Designed, Optically Tunable Gold Nanorod Dimers and Anatase TiO_2

Bryan F. Mangelson,[†,‡] Matthew R. Jones,[‡,§] Daniel J. Park,[†,‡] Chad M. Shade,[†,‡] George C. Schatz,*[,†,‡] and Chad A. Mirkin*[,†,‡,§]

[†]Department of Chemistry, [§]Department of Materials Science and Engineering, and [‡]International Institute for Nanotechnology, Northwestern University, 2145 Sheridan Road, Evanston, Illinois 60208, United States

Supporting Information

ABSTRACT: Herein we utilize on-wire lithography (OWL) to synthesize a composite plasmonic–semiconductor material composed of Au nanorod dimers embedded within anatase TiO_2 sheets. We demonstrate that, despite the harsh conditions necessary to synthesize crystalline TiO_2, the gapped nanostructures remain intact. Additionally, we show that the optical properties of these structures can be tailored via the geometric control afforded by the OWL process to produce structures with various gap sizes exhibiting different electric field intensities near the surface of the metal particles and that those fields penetrate into the semiconductor material. Finally, we show that this composite amplifies the electric field of incident light on it by a factor of 10^3, which is more that 750 times greater than the isotropic materials typically used for these systems.

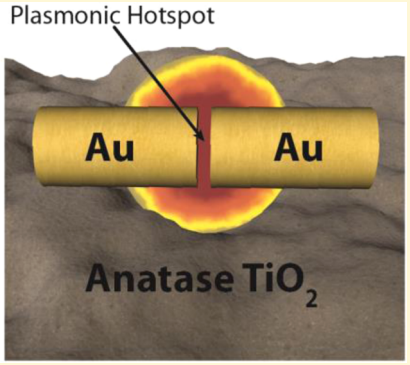

INTRODUCTION

Composite materials are created by the combination of two or more dissimilar components in such a way so as to realize new emergent properties that are not characteristic of either material individually.[1] Recently, a new class of composite materials has emerged by combining plasmonically active noble metal nanoparticles with semiconducting materials. These composites are interesting for applications in sensing,[2] photovoltaics,[3,4] and photocatalysis,[5] because of the superior optical properties derived from the combination of these two types of materials. These include an improved efficiency of absorption,[6,7] as well as an expansion of the spectral sensitivity beyond that of the native semiconductor.[8−10] An idealized composite requires (1) plasmonic nanostructures with rationally designed geometric features that are both amenable to enhancing the surrounding medium and robust with respect to the sometimes extreme conditions used to synthesize the semiconductor and (2) the ability to easily integrate such structures with a semiconductor material. The latter requires achieving the proper interface between these two dissimilar materials, which is by no means trivial, as differing chemical, mechanical, and physical properties can inhibit the proper formation of the various structures within the composite.

Herein, we report how on-wire lithography (OWL) can be used to overcome these challenges and synthesize a composite material composed of robust gold nanorod dimers, with tunable optical properties, embedded in porous sheets of anatase TiO_2.[11,12] We show that both the structure and optical properties of the gold dimers are preserved despite the harsh conditions necessary to synthesize the semiconductor component. It is further shown that the electromagnetic properties of this material can be tuned via the rational design of the gold dimers to absorb light at various wavelengths. Lastly, it is demonstrated that the composite can amplify the electric field of the light incident on it by a factor of 10^3, which is more than 750 times greater than the isotropic materials typically used for these systems.

The plasmonic character of noble metal nanoparticles is observed when they are irradiated with light and a localized surface plasmon resonance (LSPR) is excited.[13−15] This excitation involves an oscillation of the conduction electrons of the metal, which is driven by the electromagnetic field of the incident light. Additionally, an amplification of the incident electromagnetic field near the surface of a resonating plasmonic particle is observed. The precise location of these regions of intense fields, often termed hot spots, and the amplification realized within them, is highly dependent on the geometry of the nanostructure being irradiated.[16,17] Specifically, it has been demonstrated that particles containing sharp tips (such as a cube or a prism),[18,19] and to an even larger extent structures containing nanoscale gaps (optimally less than 10 nm), generate much more intense hot spots than more spherical structures.[20,21] These hot spots are important for plasmonic–semiconductor composites because it has been shown that the

Received: April 22, 2014
Revised: May 23, 2014
Published: June 5, 2014

Scheme 1. Synthesis of Nanorod Dimers Embedded in Porous Anatase TiO_2 Sheets

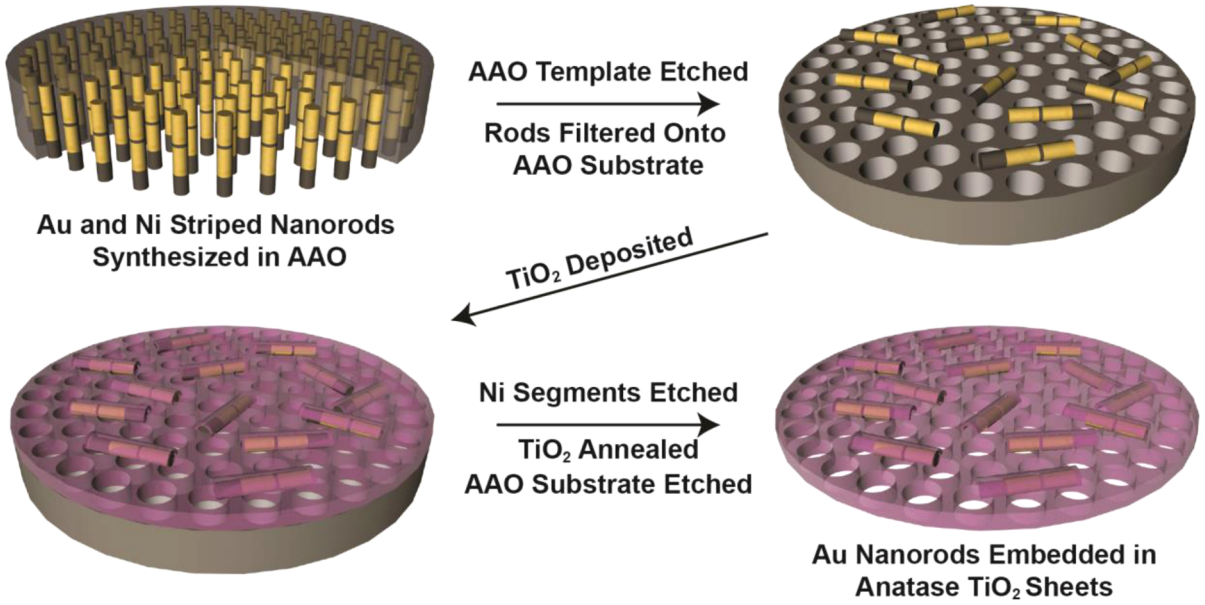

emergent photoprocesses of these materials are most active in the regions of high electromagnetic field strength.[22]

In order to synthesize plasmonic hotspots, OWL, which is a template-directed electrochemical synthesis method that allows for the synthesis of plasmonic nanostructures with sub-10 nm gaps, was used.[11,12,23] OWL is based on the deposition and subsequent immobilization of striped nanorods composed of chemically orthogonal materials (e.g., Au and Ni).[12,24] Etching of the more chemically active material (Ni) allows for the production of nanorod dimers with rationally designed geometric parameters including diameter, segment length, and gap size. This geometric control allows for precise tuning of the plasmon resonance of the final structure.[23] While OWL has already been shown to be useful for a number of applications,[25−35] including effectively creating plasmonically active noble metal dimers with very small and reproducible gaps,[11,20,23,29,36−45] it has yet to be proven useful for the synthesis of composite plasmonic and semiconductor materials.

Incorporating plasmonic structures into a semiconductor material poses multiple challenges, as it requires the coupling of two or more materials that differ significantly in their composition, phase, surface charge, and degree of interfacial epitaxy. Moreover, the geometric integrity of many plasmonic nanostructures (especially those that are anisotropic or have small gaps) can be extremely sensitive to the conditions used during fabrication, especially surface functionalization, chemical etching, and thermal annealing.

The semiconductor material often used for these types of composites is anatase TiO_2, a canonical photocatalytic material, due to its high activity, availability, chemical stability, and low toxicity.[46,47] However, room temperature syntheses of TiO_2 typically do not result in the formation of the anatase phase.[48] Therefore, after synthesis, the crystallization of anatase is necessary and requires a high-temperature annealing step for the conversion of amorphous TiO_2 to anatase.

To date, a number of different methods have been employed to synthesize these types of composite materials, but they typically do not provide much control over the morphology of the metal nanostructure, leading to the formation of roughly spherical particles.[4,10,49,50] Some examples do utilize colloidal anisotropic particles, but these methods do not allow for the formation of rationally controlled gaps.[6−8,10,51] Those few methods that do allow for the formation of gaps (often lithographically based) do so at the expense of throughput and typically cannot make features smaller than 10 nm,[9,52] which is critical for obtaining optimal plasmonic activity.

EXPERIMENTAL SECTION

In order to synthesize the plasmonic−semiconductor composite, three samples of nanorod dimers with varied gap size were prepared, followed by the deposition, annealing, and eventual liftoff of TiO_2 films, with the final product being porous sheets of anatase TiO_2 containing nanorod dimers (Scheme 1). The detailed synthesis of OWL structures has been reported previously[11,53] but will be addressed briefly herein. Anodized aluminum oxide (AAO) membranes with 35 nm pores were purchased from Synkera Technologies Inc. and used as templates for the electrodeposition of the nanorods. The AAO was first coated with 200 nm of Ag with a Kurt J. Lesker PVD 75 e-beam evaporation system and then assembled into a Teflon cell for subsequent electrochemical deposition of the rods. Ni (nickel sulfamate RTU), Au (Orotemp 24 RTU Rack), and Ag (Techni Ag Cyless II RTU) plating solutions were purchased from Technic Inc. A potentiostat utilizing a Ag/AgCl reference electrode, a Pt counter electrode, and a working electrode consisting of the Ag coated AAO was used to electroplate first a sacrificial Ag segment followed by the Au and Ni striped nanowires. The precise length of each nanowire segment was tuned by controlling the amount of charge passed though the electrochemical cell. After nanowires with the desired geometry were electrochemically synthesized, the Ag film and sacrificial segment were etched from the AAO in a 4:1:1 solution of ethanol, 30% NH_4OH (aq), and 30% H_2O_2 (aq). Subsequently, the AAO itself was etched in an aqueous 3 M NaOH solution containing 0.5 mM cetyltrimethylammonium bromide (CTAB). The CTAB surfactant was included to passivate the surface of the nanowires and impart increased colloidal stability to the resulting suspension. After etching, the nanorods were centrifuged at 10,600 relative centrifugal force (RCF) for 4 min and rinsed with a 0.5 mM CTAB solution four times.

To embed the nanowires into TiO_2 sheets, the nanowire solution was filtered through Whatman Anopore AAO membranes with a nominal pore diameter of 0.02 μm, although it was discovered that this was not the pore diameter on the surface (Figure 1d). The rod-coated membranes were then placed into an e-beam evaporation system and

dx.doi.org/10.1021/cm5014625 | Chem. Mater. 2014, 26, 3818−3824

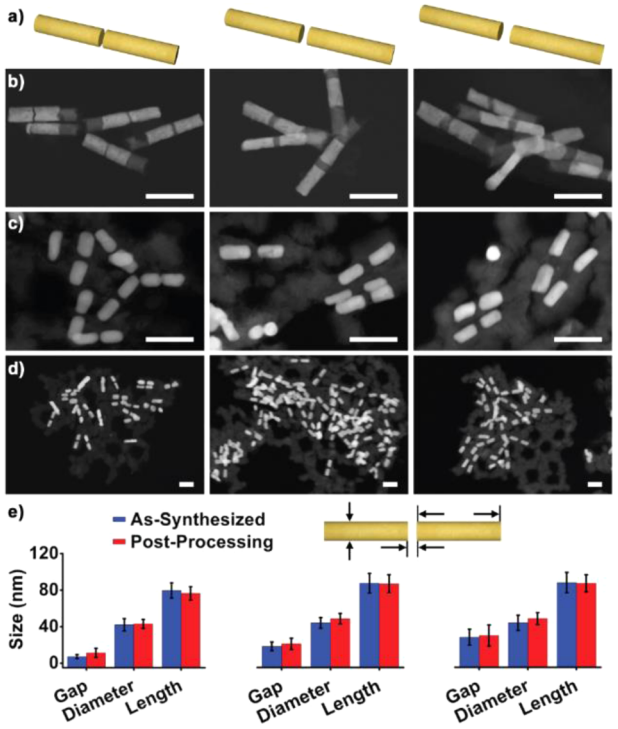

Figure 1. (a) Illustrations of the nanorod dimers with varying gap size synthesized for this work. (b) STEM images show the three sets of rod dimers just after being synthesized and removed from the AAO and (c) after embedding in TiO_2 sheets, etching the Ni segments, and annealing at elevated temperatures. (d) Wider view of dimers in annealed sheets. (e) Statistical measurements of the geometry of the dimers show that the processing conditions do not significantly change the dimer structure. (Scale bars are 150 nm.)

then coated with 80 nm of amorphous TiO_2. After removing the membranes from the evaporator, they were soaked in an aqueous solution of 3 wt % $FeCl_3$ for 30 min in order to etch the Ni segments of the rods, leaving the gold segments with programmed gap dimensions held in place by the underlying TiO_2 film. The membranes were subsequently soaked twice in DI water for 10 min to rinse away excess $FeCl_3$. Annealing of the material was carried out in an oven under ambient conditions with a ramp rate of 2.4 °C/min to a final temperature of 450 °C, which was maintained for 60 min followed by a passive slow cooling back to room temperature. The annealed TiO_2 sheets were then removed from the substrate by etching away the AAO with a 3 M NaOH aqueous solution. The resulting suspension of sheets was centrifuged and rinsed four times with DI water to remove dissolved alumina species.

Scanning transmission electron microscopy (STEM, Hitachi HD2300), energy dispersive spectroscopy (EDS), X-ray diffraction (XRD Rigaku XDS 2000), and UV−vis−NIR spectroscopy were used to probe the physical, chemical, and optical properties of the sheets, respectively.

Finite-difference time-domain (FDTD) simulations (Lumerical FDTD solutions v.8.7.0) were carried out to probe the local electromagnetic field generated by the nanorod dimer embedded in TiO_2 sheets.[54] A total field scattered field plane wave source was used to illuminate the structure, and the electric field profile was measured using a frequency-domain profile monitor. In order to closely mimic the physical structures that were synthesized, gold nanorod dimers of varying gap lengths (7, 18, and 28 nm) were simulated having an 80 nm thick semicircular shell of anatase TiO_2. Additionally, FDTD simulations were carried out on various other geometries of plasmonic particles, including an isolated gold rod segment and a 10 nm gold sphere. This allows for comparison between the gapped nanostructure used in this work and plasmonic structures that are similar to those used in the past for these types of composite materials.[8−10,51] The dielectric functions of Au[55] and TiO_2[56] were taken from experimental data. All structures were simulated in a water environment with a refractive index of 1.33.

RESULTS AND DISCUSSION

Because the synthetic method described herein utilizes high temperature annealing in addition to chemical etching and a lift-off step, it is not obvious that the structural integrity and, by extension, the optical activity of the OWL dimers would remain intact. It was therefore necessary to demonstrate that the structural features of the nanorod dimers (with gaps as small as ∼7 nm) were preserved during the fabrication process, despite these extreme conditions. To do this we analyzed the physical, chemical, and optical properties of the sheet materials throughout the fabrication process. First, STEM images were collected on each of three sets of nanorod dimers with different gap sizes just after synthesis of the striped nanorods and after the processing involved in the formation of the dimer-embedded anatase sheets. This was done to understand the impact of the harsh thermal treatment on the structural integrity of the features programmed into the nanorods during the electrochemical synthesis (Figure 1). It was observed that the geometry of the dimers changed only slightly compared to their as-synthesized dimensions as a result of the annealing, etching, and lift-off procedures. Specifically, the diameter, gap size, and segment length of the nanorod dimers remained unchanged (Figure 1e), but a slight rounding of the rod segments was observed, which can be understood by the diffusion of gold surface atoms at elevated temperatures. A wider view of the material shows the discrete nature of sheets, and that the porous structure of the anodized aluminum oxide (AAO), which was used as the substrate for the deposition, was transferred to the TiO_2 (Figure 1d). AAO was selected as the substrate to work with for three reasons: (1) Because of its porous nature, the AAO acts as a nanoscale filter for collecting the colloidal solution of rods on a substrate while minimizing aggregation associated with drying effects (though the microscopy images show that there is still some amount of random aggregation of the dimers, which has consequences for the optical properties of the final material), (2) AAO is chemically inert with respect to the conditions necessary for Ni etching and also stable at the temperatures necessary for the annealing of TiO_2, and (3) the ability to selectively etch the AAO after processing leaves the gold nanorod dimer-embedded TiO_2 sheets intact and solution dispersible.

Although the TEM results demonstrate preservation of the nanorod dimer morphology, they do not provide compositional information on either the plasmonic structures or the TiO_2 sheets in which they are embedded. To probe this, compositional mapping using energy dispersive spectroscopy (EDS) was performed on the synthesized films to measure the nanoscale elemental distribution in the samples (Figure 2a). From these results, it is obvious that the dimer structures remain Au and the underlying substrate is primarily Ti, with minimal mixing between the two. The lack of mixing is critical to the formation of the anatase phase, and also the optical properties of the gold, and is not at all a foregone conclusion at these temperatures. In fact, we have shown that Ni and Au diffuse together under these conditions. This has the effect of removing the gap between the gold structures. It is for this reason that during the synthesis the Ni is etched prior to annealing. (Supporting Information Figure S1).

dx.doi.org/10.1021/cm5014625 | Chem. Mater. 2014, 26, 3818−3824

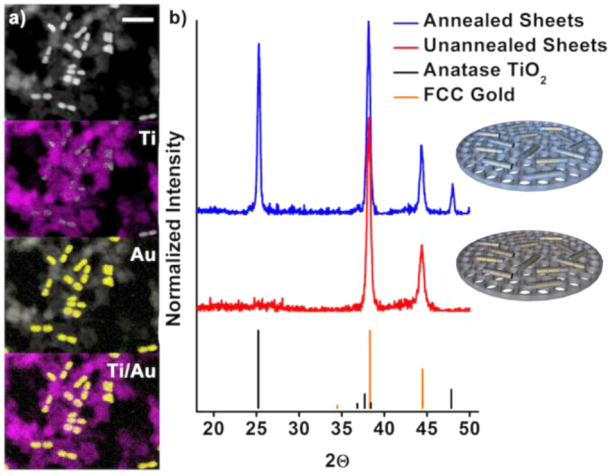

Figure 2. (a) STEM image and EDS maps of nanorod dimers embedded in TiO_2. Signal from Ti is shown in pink and Au in yellow. Scale bar is 300 nm. (b) XRD data on annealed (blue trace) and unannealed (red trace) sheets. Standard peak locations for anatase TiO_2 and FCC gold are shown for reference.

The EDS data provide detailed compositional information as a function of spatial distribution, but it does not provide information on the crystalline structure of either part of the hybrid material. To characterize the phase of the Au and Ti components found in the EDS measurements, powder X-ray diffraction (XRD) was used to compare the crystal structure and degree of crystallinity of hybrid films before and after annealing[57] (Figure 2b). First, peaks that are diagnostic of the presence of FCC gold were observed regardless of annealing conditions, confirming the preservation of the crystallinity of the Au plasmonic nanorod dimers. Second, strong reflections indicative of anatase TiO_2 were observed in the hybrid material only after having been taken through the thermal annealing step (blue trace, annealed sheets, Figure 2b). Taken together, these observations confirm the ability to synthesize the photoactive anatase phase of TiO_2 while maintaining the gold rod crystallinity and morphology within the film.

In order to probe whether the plasmonic properties of the nanorod dimers are preserved while embedding and during the subsequent Ni etching, TiO_2 annealing, and the final lift off process, the sheets were dispersed in aqueous solutions for

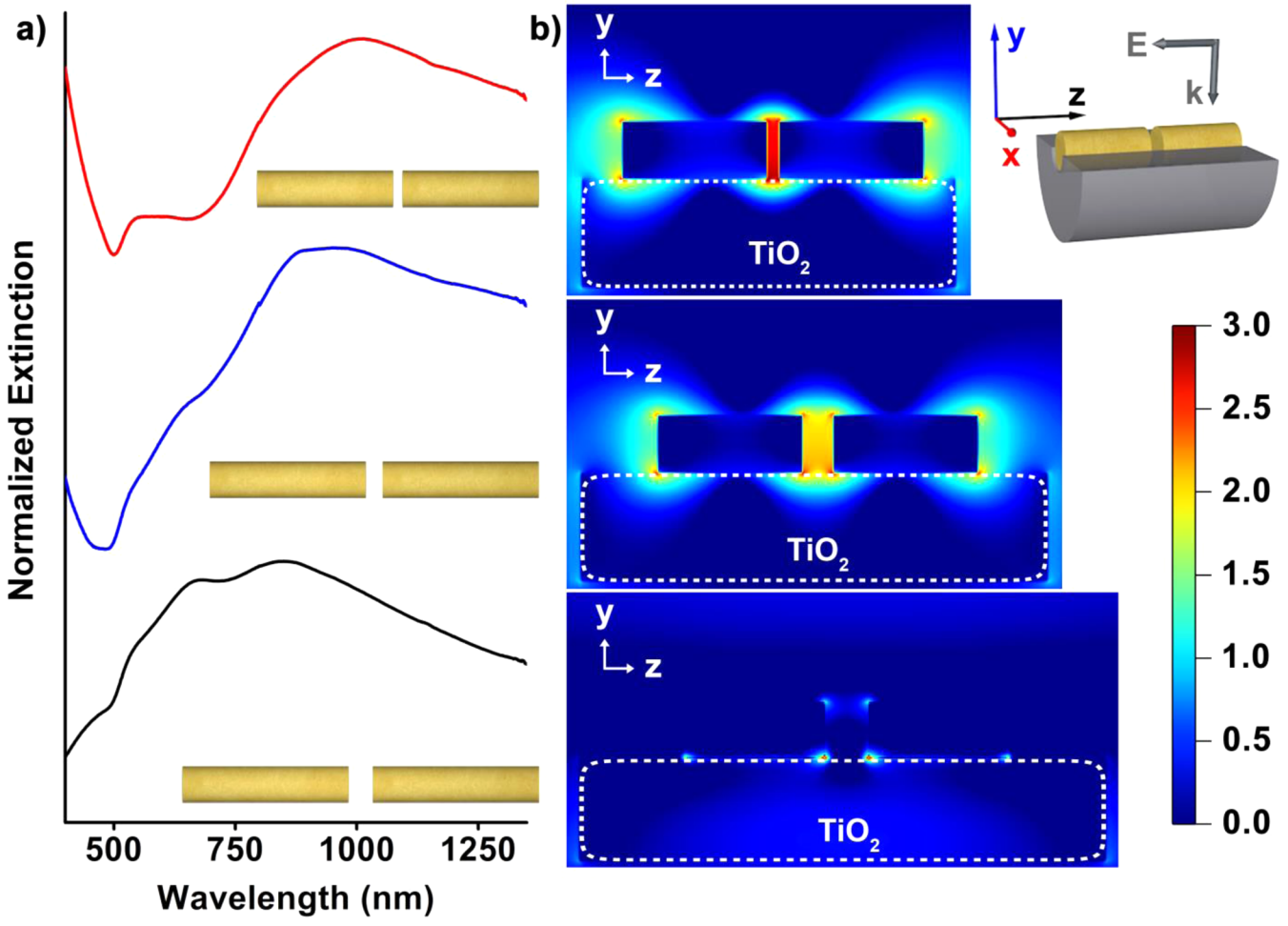

Figure 3. (a) Normalized UV−vis−NIR spectra for plasmonic dimers with differing gap sizes embedded in sheets of anatase TiO_2 in water. Spectra were obtained by subtracting a solution containing only TiO_2 sheets as a background. It can be seen that as the gaps get larger the plasmon resonance of the structures blue-shift. (b) FDTD electric field intensity maps of gold nanorod dimers that are 43 nm in diameter, have gaps between dimer segments of 7, 18, and 28 nm, and are coated with a half shell of 80 nm thick anatase TiO_2 (see inset). The plots show the intensity of the field at the resonances for each dimer, which are 1100, 1050, and 1030 nm, respectively. It is observed that as the gap becomes larger the electric field intensity decreases, showing the tunability available using this system. Additionally it can be seen that the electric field penetrates well into the semiconductor material. Electric field intensities are plotted on a log scale where zero is equal to the intensity of the incident field.

dx.doi.org/10.1021/cm5014625 | *Chem. Mater.* 2014, 26, 3818−3824

UV−vis−NIR spectroscopic characterization (Figure 3a). The results confirm that the position of the dipole plasmon resonance shifts with increased coupling between rod segments as a result of the changing gap size. This trend is expected and important because it shows that the rationally designed nanometer-scale gap distances programmed into each structure and the consequent localized electromagnetic fields are preserved on average in each sample. It is also important to note that the large breadth of the peaks in the UV−vis−NIR measurement do not reflect the spectral response of an individual nanorod dimer. Peak broadening in this ensemble measurement is likely due to a number of contributing factors, including the polydispersity of the dimers as a result of both the initial syntheses and the subsequent rounding after annealing, the excitation of higher order plasmonic modes that are similar in energy to the dipolar resonance, and transverse and/or longitudinal coupling between neighboring nanorod dimers due to their proximity within sheets as a result of random aggregation processes.

To further explore the optical properties of this material, FDTD simulations were used to characterize the localized electric field for the various dimer geometries when embedded within anatase TiO_2 (Figure 3b). The field intensity profiles clearly demonstrate that the electric field localized by these particles is highly dependent on the size of the gap between rod segments. This means that the nanoscale tailorability in the size of the gap afforded by this synthesis methodology is directly correlated with an extraordinary tailorability in the intensity of the electric field resulting from the plasmonic excitation of these dimer structures. Additionally, it is clear from the simulations that the intense fields generated by the plasmonic coupling of the rod segments penetrate several tens of nanometers into the semiconductor material, which should provide significant enhancement to the photoprocesses taking place therein. These characteristics that result from synthetic control demonstrate the potential of this system to be used as a platform for the systematic study of the impact of localized electric field intensity on the photoactivity of these types of hybrid plasmonic semiconductor systems.

In most of the previous examples of these types of materials, the plasmonic components used are spheres or sphere-like particles.[4,6,7,10,49,50] Additionally, there are some examples of anisotropic plasmonic particles being interfaced with the semiconductor materials.[6−10,22,51,58] To compare the plasmonic response of the gapped nanostructures utilized in this work to particles common in the literature, additional FDTD simulations were carried out on an isolated gold rod segment and a spherical gold nanoparticle. By plotting the electric field intensity of these structures and the gapped dimer on the same scale, a fair side-by-side comparison of the hot spots generated by each structure can be made (Figure 4). The field plots of these particles clearly show that the gapped structure generates fields that are almost 3 orders of magnitude greater than those of the sphere ($1 \times 10^{3.16}$ vs $1 \times 10^{0.27}$) and about 50 times greater than that of the rod segment alone ($1 \times 10^{1.49}$). Also, when considering not just the peak intensity of the respective fields but also the volume enhanced by each structure, the gapped structure is seen to be far superior to the other geometries. This result indicates that composite plasmonic−semiconductor materials that incorporate gapped structures have the potential to be far superior to those that do not.

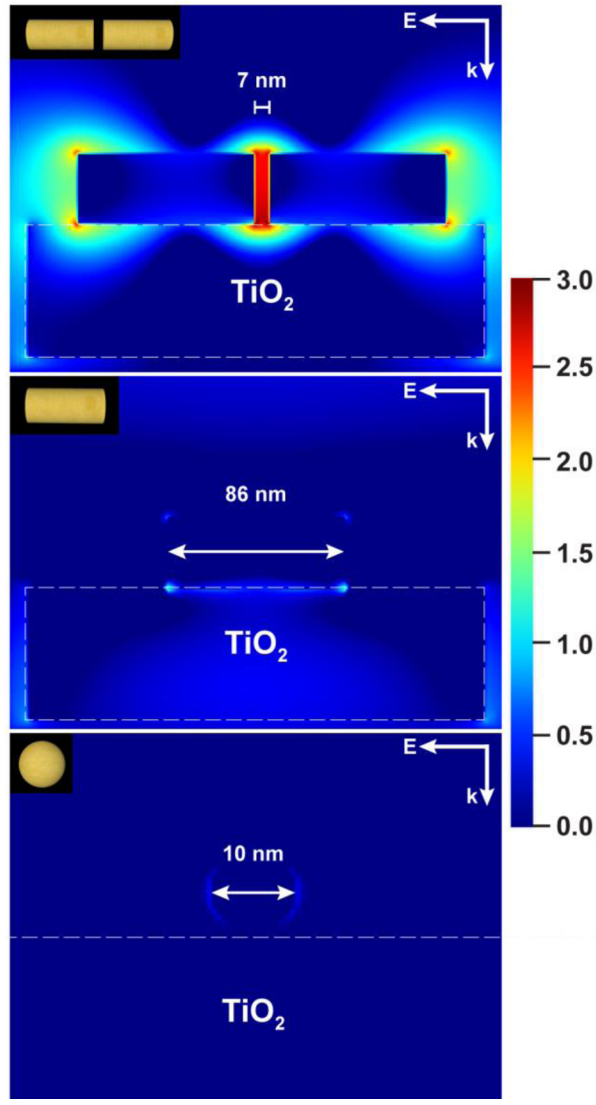

Figure 4. FDTD electric field plots for a Au nanorod dimer 43 nm in diameter with two 86 nm segments separated by a 7 nm gap (top), a single isolated Au nanorod segment with the same dimensions as the ones above (middle), and a spherical Au nanoparticle 10 nm in diameter (bottom). The intensity map is plotted at the plasmon resonance for each structure, which is 1100, 952, and 565 nm, respectively. The insets are cartoon representations of the structures modeled. Electric field intensities are plotted on a log scale where zero is equal to the intensity of the incident field.

■ CONCLUSION

In this work we have developed a procedure for synthesizing gold nanorod dimers embedded within anatase TiO_2 sheets as a case study for the incorporation of plasmonically active materials into generic semiconductor films. Despite the harsh conditions necessary to crystallize photoactive TiO_2, the morphology and crystallinity of plasmonic dimers are both sufficiently preserved so as to maintain a high degree of tunability in the plasmon resonance and electromagnetic field distribution within the gap. This technique will serve as a platform for systematic studies of the impact of the local electric field enhancement generated by plasmonic structures on light-based sensitization processes within semiconductors. In addition, it can serve as a generalizable approach for synthesizing myriad composite plasmonic−semiconductor

dx.doi.org/10.1021/cm5014625 | Chem. Mater. 2014, 26, 3818−3824

materials by incorporating a variety of strongly enhancing plasmonic nanostructures into various photoactive semiconductors.

■ ASSOCIATED CONTENT

Supporting Information

Further characterization. This material is available free of charge via the Internet at http://pubs.acs.org.

■ AUTHOR INFORMATION

Corresponding Authors

*E-mail: chadnano@northwestern.edu (C.M.S.).
*E-mail: g-schatz@northwestern.edu (G.C.S.).

Notes

The authors declare no competing financial interest.

■ ACKNOWLEDGMENTS

This material is based upon work supported by the AOARD under Award No. FA2386-13-1-4124, the Nonequilibrium Energy Research Center (NERC), an Energy Frontier Research Center funded by the U.S. Department of Energy/Office of Science/Office of Basic Energy Sciences Award DE-SC0000989, the Office of the Asst. Secr. of Defense for Research and Engineering/NSSEFF Program/Naval Postgraduate School Awards N00244-09-1-0012 and N00244-09-1-0071. M.R.J. is grateful to the NSF for a Graduate Research Fellowship. This work made use of the EPIC facility (NUANCE Center—Northwestern University) and the J.B. Cohen X-ray Diffraction Facility, which have received support from the MRSEC program (NSF DMR-1121262) at the Materials Research Center and the Nanoscale Science and Engineering Center (EEC-0118025/003), both programs of the National Science Foundation.

■ ABBREVIATIONS

OWL, on-wire lithography; LSPR, localized surface plasmon resonance; RCF, relative centrifugal force; CTAB, cetyltrimethylammonium bromide; STEM, scanning transmission electron microscopy; EDS, energy dispersive spectroscopy; XRD, X-ray diffraction; FDTD, finite-difference time domain

■ REFERENCES

(1) Rajeshwar, K.; de Tacconi, N. R.; Chenthamarakshan, C. R. *Chem. Mater.* **2001**, *13*, 2765.
(2) Knight, M. W.; Sobhani, H.; Nordlander, P.; Halas, N. J. *Science* **2011**, *332*, 702.
(3) Atwater, H. A.; Polman, A. *Nat. Mater.* **2010**, *9*, 205.
(4) Tian, Y.; Tatsuma, T. *J. Am. Chem. Soc.* **2005**, *127*, 7632.
(5) Linic, S.; Christopher, P.; Ingram, D. B. *Nat. Mater.* **2011**, *10*, 911.
(6) Ingram, D. B.; Christopher, P.; Bauer, J. L.; Linic, S. *ACS Catal.* **2011**, *1*, 1441.
(7) Ingram, D. B.; Linic, S. *J. Am. Chem. Soc.* **2011**, *133*, 5202.
(8) Lee, J.; Mubeen, S.; Ji, X.; Stucky, G. D.; Moskovits, M. *Nano Lett.* **2012**, *12*, 5014.
(9) Nishijima, Y.; Ueno, K.; Yokota, Y.; Murakoshi, K.; Misawa, H. *J. Phys. Chem. Lett.* **2010**, *1*, 2031.
(10) Pu, Y.-C.; Wang, G.; Chang, K.-D.; Ling, Y.; Lin, Y.-K.; Fitzmorris, B. C.; Liu, C.-M.; Lu, X.; Tong, Y.; Zhang, J. Z.; Hsu, Y.-J.; Li, Y. *Nano Lett.* **2013**, *13*, 3817.
(11) Osberg, K. D.; Schmucker, A. L.; Senesi, A. J.; Mirkin, C. A. *Nano Lett.* **2011**, *11*, 820.
(12) Qin, L. D.; Park, S.; Huang, L.; Mirkin, C. A. *Science* **2005**, *309*, 113.
(13) Jones, M. R.; Osberg, K. D.; Macfarlane, R. J.; Langille, M. R.; Mirkin, C. A. *Chem. Rev.* **2011**, *111*, 3736.
(14) Kelly, K. L.; Coronado, E.; Zhao, L. L.; Schatz, G. C. *J. Phys. Chem. B* **2003**, *107*, 668.
(15) Schuller, J. A.; Barnard, E. S.; Cai, W. S.; Jun, Y. C.; White, J. S.; Brongersma, M. L. *Nat. Mater.* **2010**, *9*, 193.
(16) Murphy, C. J.; San, T. K.; Gole, A. M.; Orendorff, C. J.; Gao, J. X.; Gou, L.; Hunyadi, S. E.; Li, T. *J. Phys. Chem. B* **2005**, *109*, 13857.
(17) Schatz, G. C. *Acc. Chem. Res.* **1984**, *17*, 370.
(18) Rycenga, M.; Langille, M. R.; Personick, M. L.; Ozel, T.; Mirkin, C. A. *Nano Lett.* **2012**, *12*, 6218.
(19) Verhagen, E.; Polman, A.; Kuipers, L. *Opt. Express* **2008**, *16*, 45.
(20) Qin, L.; Zou, S.; Xue, C.; Atkinson, A.; Schatz, G. C.; Mirkin, C. A. *Proc. Natl. Acad. Sci. U. S. A.* **2006**, *103*, 13300.
(21) Willingham, B.; Brandl, D. W.; Nordlander, P. *Appl. Phys. B-Lasers O.* **2008**, *93*, 209.
(22) Kazuma, E.; Sakai, N.; Tatsuma, T. *Chem. Commun.* **2011**, *47*, 5777.
(23) Mangelson, B. F.; Park, D. J.; Ku, J. C.; Osberg, K. D.; Schatz, G. C.; Mirkin, C. A. *Small* **2013**, *9*, 2250.
(24) Nicewarner-Pena, S. R.; Freeman, R. G.; Reiss, B. D.; He, L.; Pena, D. J.; Walton, I. D.; Cromer, R.; Keating, C. D.; Natan, M. J. *Science* **2001**, *294*, 137.
(25) Chen, X.; Jeon, Y. M.; Jang, J. W.; Qin, L.; Huo, F.; Wei, W.; Mirkin, C. A. *J. Am. Chem. Soc.* **2008**, *130*, 8166.
(26) Chen, X. D.; Braunschweig, A. B.; Wiester, M. J.; Yeganeh, S.; Ratner, M. A.; Mirkin, C. A. *Angew. Chem., Int. Ed.* **2009**, *48*, 5178.
(27) Chen, X. D.; Yeganeh, S.; Qin, L. D.; Li, S. Z.; Xue, C.; Braunschweig, A. B.; Schatz, G. C.; Ratner, M. A.; Mirkin, C. A. *Nano Lett.* **2009**, *9*, 3974.
(28) Chen, X. D.; Zheng, G. F.; Cutler, J. I.; Jang, J. W.; Mirkin, C. A. *Small* **2009**, *5*, 1527.
(29) Ozel, T.; Bourret, G. R.; Schmucker, A. L.; Brown, K. A.; Mirkin, C. A. *Adv. Mater.* **2013**, *25*, 4515.
(30) Qin, L. D.; Banholzer, M. J.; Xu, X. Y.; Huang, L.; Mirkin, C. A. *J. Am. Chem. Soc.* **2007**, *129*, 14870.
(31) Qin, L. D.; Jang, J. W.; Huang, L.; Mirkin, C. A. *Small* **2007**, *3*, 86.
(32) Schmucker, A. L.; Barin, G.; Brown, K. A.; Rycenga, M.; Coskun, A.; Buyukcakir, O.; Osberg, K. D.; Stoddart, J. F.; Mirkin, C. A. *Small* **2013**, *9*, 1900.
(33) Zheng, G. F.; Chen, X. D.; Mirkin, C. A. *Small* **2009**, *5*, 2537.
(34) Zheng, G. F.; Qin, L. D.; Mirkin, C. A. *Angew. Chem., Int. Ed.* **2008**, *47*, 1938.
(35) Zhou, X. Z.; Shade, C. M.; Schmucker, A. L.; Brown, K. A.; He, S.; Boey, F.; Ma, J.; Zhang, H.; Mirkin, C. A. *Nano Lett.* **2012**, *12*, 4734.
(36) Banholzer, M. J.; Osberg, K. D.; Li, S.; Mangelson, B. F.; Schatz, G. C.; Mirkin, C. A. *ACS Nano* **2010**, *4*, 5446.
(37) Bourret, G. R.; Ozel, T.; Blaber, M.; Shade, C. M.; Schatz, G. C.; Mirkin, C. A. *Nano Lett.* **2013**, *13*, 2270.
(38) Osberg, K. D.; Rycenga, M.; Bourret, G. R.; Brown, K. A.; Mirkin, C. A. *Adv. Mater.* **2012**, *24*, 6065.
(39) Osberg, K. D.; Rycenga, M.; Harris, N.; Schmucker, A. L.; Langille, M. R.; Schatz, G. C.; Mirkin, C. A. *Nano Lett.* **2012**, *12*, 3828.
(40) Qin, L.; Banholzer, M. J.; Millstone, J. E.; Mirkin, C. A. *Nano Lett.* **2007**, *7*, 3849.
(41) Schmucker, A. L.; Dickerson, M. B.; Rycenga, M.; Mangelson, B. F.; Brown, K. A.; Naik, R. R.; Mirkin, C. A. *Small* **2014**, *10*, 1485.
(42) Schmucker, A. L.; Harris, N.; Banholzer, M. J.; Blaber, M. G.; Osberg, K. D.; Schatz, G. C.; Mirkin, C. A. *ACS Nano* **2010**, *4*, 5453.
(43) Wei, W.; Li, S.; Millstone, J. E.; Banholzer, M. J.; Chen, X.; Xu, X.; Schatz, G. C.; Mirkin, C. A. *Angew. Chem., Int. Ed.* **2009**, *48*, 4210.
(44) Wei, W.; Li, S.; Qin, L.; Xue, C.; Millstone, J. E.; Xu, X.; Schatz, G. C.; Mirkin, C. A. *Nano Lett.* **2008**, *8*, 3446.
(45) Zhou, X.; Zhou, Y.; Ku, J. C.; Zhang, C.; Mirkin, C. A. *ACS Nano* **2014**, *8*, 1511.
(46) Konstantinou, I. K.; Albanis, T. A. *Appl. Catal., B* **2004**, *49*, 1.
(47) Linsebigler, A. L.; Lu, G.; Yates, J. T. *Chem. Rev.* **1995**, *95*, 735.

(48) Hanaor, D. H.; Sorrell, C. *J. Mater. Sci.* **2011**, *46*, 855.
(49) Kumar, M. K.; Krishnamoorthy, S.; Tan, L. K.; Chiam, S. Y.; Tripathy, S.; Gao, H. *ACS Catal.* **2011**, *1*, 300.
(50) Zhou, J.; Ren, F.; Zhang, S.; Wu, W.; Xiao, X.; Liu, Y.; Jiang, C. *J. Mater. Chem. A* **2013**, *1*, 13128.
(51) Mubeen, S.; Lee, J.; Singh, N.; Kramer, S.; Stucky, G. D.; Moskovits, M. *Nat. Nanotechnol.* **2013**, *8*, 247.
(52) Salmistraro, M.; Schwartzberg, A.; Bao, W.; Depero, L. E.; Weber-Bargioni, A.; Cabrini, S.; Alessandri, I. *Small* **2013**, *9*, 3301.
(53) Banholzer, M. J.; Qin, L.; Millstone, J. E.; Osberg, K. D.; Mirkin, C. A. *Nat. Protoc.* **2009**, *4*, 838.
(54) Taflove, A.; Hagness, S. C. *Computational electrodynamics: the finite-difference time-domain method*; Artech House: Boston, 2005.
(55) Johnson, P. B.; Christy, R. W. *Phys. Rev. B* **1972**, *6*, 4370.
(56) Kim, S. Y. *Appl. Opt.* **1996**, *35*, 6703.
(57) Standridge, S. D.; Schatz, G. C.; Hupp, J. T. *Langmuir* **2009**, *25*, 2596.
(58) Ide, Y.; Matsuoka, M.; Ogawa, M. *J. Am. Chem. Soc.* **2010**, *132*, 16762.